Salt-Induced Conformation and Interaction Changes of Nucleosome Core Particles

Stéphanie Mangenot,* Amélie Leforestier,* Patrice Vachette,† Dominique Durand,† and Françoise Livolant*
*Laboratoire de Physique des Solides, Bât 510, Université Paris-Sud, 91405 Orsay Cedex, France; and †Laboratoire pour l'Utilisation du Rayonnement Electromagnétique, Bât 209D, Université Paris-Sud, BP 34, 91898 Orsay Cedex, France

ABSTRACT Small angle x-ray scattering was used to follow changes in the conformation and interactions of nucleosome core particles (NCP) as a function of the monovalent salt concentration C_s. The maximal extension (D_{max}) of the NCP (145 ± 3-bp DNA) increases from 137 ± 5 Å to 165 ± 5 Å when C_s rises from 10 to 50 mM and remains constant with further increases of C_s up to 200 mM. In view of the very weak increase of the R_g value in the same C_s range, we attribute this D_{max} variation to tail extension, a proposal confirmed by simulations of the entire $I(q)$ curves, considering an ideal solution of particles with tails either condensed or extended. This tail extension is observed at higher salt values when particles contain longer DNA fragments (165 ± 10 bp). The maximal extension of the tails always coincides with the screening of repulsive interactions between particles. The second virial coefficient becomes smaller than the hard sphere virial coefficient and eventually becomes negative (net attractive interactions) for NCP_{145}. Addition of salt simultaneously screens Coulombic repulsive interactions between NCP and Coulombic attractive interactions between tails and DNA inside the NCP. We discuss how the coupling of these two phenomena may be of biological relevance.

INTRODUCTION

Both histone-fold DNA interactions in the core particle and histone tails interactions in chromatin are thought to contribute to repression of chromatin expression (Kornberg and Lorch, 1999). Each of these levels of repression can be counterbalanced by specific mechanisms, leading to structural transitions inside the nucleosome core particle and also in their supramolecular organization. However, progresses in understanding mechanisms that regulate chromatin dynamics is limited by the lack of structural data regarding 1) the conformational changes of the nucleosome core particle and 2) the overall organization of chromatin. At both levels, conformational changes are expected to occur in response to slight changes in the local environment. These may be changes in salt concentration and pH and possible interactions with different molecules (multivalent ions or proteins for example). Electrostatic effects are known to play a central role in the stability of the nucleosome and also in the condensation of the fiber. Because electrostatics effects can be modulated by acting on salt concentration, systematic variation of the type and concentration of the salt in the milieu provides a way to explore the stability of the nucleosome particles and to monitor their interactions.

First, the nucleosome core particle contains the histone octamer core with two each of the core histones H2A, H2B, H3, and H4 and 146 to 147 bp of DNA wrapped in a left handed helix at the surface of the protein core (Richmond et al., 1984; Lüger et al., 1997, Harp et al., 2000). The global shape of the particle is that of a flat cylinder, which diameter (105 Å) is approximately twice its height (57 Å). Histones amino terminal tails pass over and between the gyres of the DNA superhelix. The electron density for further tail sequences is weak and therefore not interpreted by crystallography. Histone tails once having left the confines of the DNA supercoil, could either remain in apparent loose association with the outside of the DNA supercoil or extend away from the nucleosome core and become rapidly disordered (Lüger and Richmond, 1998). In solution, a number of salt-induced instabilities have been reported, among which are changes in the conformation of the histone tails, for monovalent salt concentrations ranging from 0.01 to 0.4 M NaCl (Ausio et al., 1984), where the particle is considered to remain stable.

Second, the supramolecular organization of the nucleosome core particles is also highly dependent on ionic conditions. Isolated nucleosome core particles form crystalline and liquid crystalline phases at concentrations covering the concentrations of the living cell. Well-defined concentrations of monovalent cations plus small amounts of multivalent ions are required to get good diffracting crystals, which prevents the exploration of large ranges of ionic conditions. This limitation can be bypassed by studying the liquid crystalline states; a sequence of different phases has been found while increasing the salt concentration from a few millimolars up to 150 mM NaCl: a lamellar phase (Leforestier et al., 2001), a poorly ordered phase, a two-dimensional columnar phase, and a three-dimensional hexagonal crystalline phase (Leforestier and Livolant, 1997; Livolant and Leforestier, 2000; S. Mangenot, A. Leforestier, D. Durand, and F. Livolant, in preparation), all formed by columns of stacked nucleosome core particles (NCP). It is also well known that the nucleosomic filament (in which

Received for publication 17 May 2001 and in final form 24 September 2001.

Address reprint requests to Françoise Livolant, Laboratoire de Physique des Solides, Bât 510, Université Paris-Sud, 91405 Orsay Cedex, France. Tel.: 33-1-69-155392; Fax: 33-1-69-156086; E-mail: livolant@lps.u-psud.fr.

0006-3495/02/01/345/12 $2.00

nucleosome core particles are connected together by linker DNA) appears either under unfolded, condensed, or aggregated forms depending on the ionic conditions of the solution in which chromatin is extracted out of the cell (Widom, 1986). Although the presence of the fifth histone H1 is not required to follow this in vitro salt-induced condensation of the fiber, the presence of the histone tails is absolutely crucial (Garcia-Ramirez et al., 1992; Fletcher and Hansen, 1996).

Histone tails appear to be involved in the conformational changes of the nucleosome core particle and also in the structural phase transitions occurring at the supramolecular level. It is generally accepted that these tails interact with DNA at low salt and are extended outside of the particle at salt concentrations above ~0.2 M monovalent salt. However, a clear description of this process is lacking despite the number of reports on this question (Cary et al., 1978; Walker, 1984; Ausio et al., 1984, 1989; Garcia-Ramirez et al., 1992; Fletcher and Hansen, 1995, 1996; Hilliard et al., 1986; Smith and Rill, 1989; De Lucia et al., 1999; Dong et al., 1990; Ballestar and Franco, 1997; Wang et al., 2000). The difficulty comes from the heterogeneity in the samples used in the experiments (isolated nucleosome core particles with varying lengths of associated DNA, chromatin fragments, or nucleosomal arrays), and from differences in conditions of temperature and concentration under which experiments were conducted. Moreover, the methods of investigation have been extremely diverse: nuclear magnetic resonance, analytical ultracentrifugation, circular dichroïsm, x-ray and neutron scattering, and indirect methods based on cross-linking experiments. More important, the extremely large explored range of salt concentration has not always been investigated in detail. Therefore, multiple effects may sometimes superimpose (Yager et al., 1989).

We present here a careful analysis of the extension process of isolated NCP tails as a function of ionic strength, restricting ourselves to NaCl, a monovalent salt. Small angle x-ray scattering (SAXS) methods were chosen to get simultaneously the two sets of information we are interested in: 1) conformational changes in the nucleosome core particle and 2) interactions between the particles. Moreover, we tested the effects of the DNA length associated to these properties.

MATERIALS AND METHODS

NCP isolation

Nucleosome core particles were prepared from two different sources, either calf thymus or chicken erythrocytes. In both cases, chromatin was extracted in low ionic strength buffer after micrococcal nuclease digestion of nuclei. After removal of linker histones, NCP were obtained by controlled digestion with micrococcal nuclease and purified by chromatography over a Sephacryl S300 HR column (Pharmacia Biotech, Uppsala, Sweden). The mononucleosome fraction was extensively dialyzed against 10 mM Tris-EDTA (TE) buffer at a concentration of 1 to 3 mg/ml and further concentrated by ultrafiltration in a pressurized cell (model 8003, Amicon, Beverly, MA) through a hydroxypropylcellulose membrane (model YM100, Amicon) to a final concentration of 50 to 150 mg/ml. These stock solutions were stored at 0°C. To prevent proteolysis of the histone tails, 0.5 mM phenylmethylsulfonyl fluoride was added to buffers at all steps of the preparation procedure.

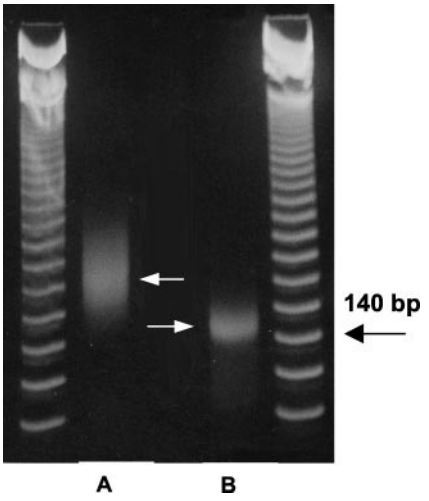

FIGURE 1 Characterization of the DNA length in the two populations of NCP prepared for these experiments: 165 ± 10 bp (from calf thymus, *A*) and 145 ± 3 bp (from chicken erythrocytes, *B*). Electrophoresis was performed on 7.5% polyacrylamide gel, and gels were stained with ethidium bromide.

Characterization of nucleosome core particles

The integrity of the NCP and the absence of contaminating di- and oligo-nucleosomes were checked by electrophoresis on 7.5% polyacrylamide gels under nondenaturing conditions. Fifteen percent sodium dodecyl sulfate-polyacrylamide gel electrophoresis was used to check the histone composition. The length of DNA associated to the protein core was determined after DNA extraction by 12% polyacrylamide gel electrophoresis and by comparison with 123 and 10 basepairs (bp) ladder DNA (Life Technologies/Gibco-BRL, Cleveland, OH). Two NCP populations were prepared for the present study, differing in the length of the DNA fragment associated to the protein core: 145 ± 3 bp (prepared from chicken erythrocytes) and 165 ± 10 bp (prepared from calf thymus) (Fig. 1). The two NCP populations will hereafter be referred to as NCP_{145} and NCP_{165}, respectively.

Sample preparation

Series of samples covering a large range of added monovalent salt concentrations (C_s) were prepared. The C_s values take into account $Tris^+$ and Na^+ cations.

For NCP_{165}, the initial stock solution (150 mg/ml NCP in 10 + 5 mM NaCl mM TE, pH 7.6) was diluted to C_{NCP} = 1 mg/ml and dialyzed against different buffers: 10 mM TE, 10 mM TE + 5 mM NaCl, 10 mM TE + 440 mM NaCl, 10 mM TE + 1000 mM NaCl to reach the final 10, 15, 450, and 1010 mM values. Other C_s values (50 and 160 mM) were obtained by addition of NaCl to the solution of NCP dialyzed against 10 mM TE + 5 mM NaCl. Each solution was then concentrated by ultrafiltration to C_{NCP} = 150 mg/ml. Final NCP concentrations (5, 10, 20, 50, 100, 150 mg/ml) were obtained by dilution in the corresponding buffer. NCP concentrations were determined by ultraviolet absorbance at 260 nm, using A_{260} = 9.5 $cm^2\ mg^{-1}$ (Ausio et al., 1984).

For NCP_{145}, the initial stock solution (50 mg/ml NCP in 10 mM TE, pH 7.6) was diluted in 10 mM TE buffer, eventually supplemented with NaCl, to adjust the final NCP concentrations to 0.5, 1, 2, and 4 mg/ml and the final C_s values to 10, 25, 37.5, 50, 75, 100, 150, and 200 mM. To minimize the errors in the salt and NCP concentrations, all dilutions were performed by weighing the samples.

SAXS measurements

Small angle x-ray scattering were carried out using the radiation synchrotron source DCI at LURE (Orsay, France) on station D 24. A bent Ge (111) monochromator is used to select the wavelength 1.488 Å, (Ni K-absorption edge). The detector was a linear position-sensitive gas detector. In the first series of experiments (NCP_{165}), the sample to detector distance was $D = 1827$ mm, corresponding to the scattering vector range 9.3×10^{-3} Å$^{-1} < q < 0.197$ Å^{-1}, in which $q = (4\pi/\lambda)\sin\theta$, with 2θ being the scattering angle. In the second series of experiments (NCP_{145}), the sample to detector distance was $D = 1892$ mm and the scattering vector range was 1.34×10^{-2} Å$^{-1} < q < 0.188$ Å^{-1}. Samples were placed in a quartz capillary ~1.5 mm in diameter. Successive frames of 200 s each were recorded at room temperature. Buffer was exposed during eight frames. To avoid any x-ray damage on NCP, each NCP solution was exposed only during four frames of 200 s. To improve data statistics, the acquisition was repeated two, three, or four times after moving fresh solution into the beam. Each frame was then carefully inspected to check for radiation damage. None was found. The intensity curves were scaled to the transmitted beam intensity before background subtraction.

Data analysis

For a solution of noninteracting identical particles, the scattering intensity can be expanded in powers of q at small q values according to the well known Guinier approximation (Guinier and Fournet, 1955):

$$I(q) = I(0)\exp\left(-\frac{q^2R_g^2}{3}\right) \quad (1)$$

in which R_g is the radius of gyration of the particle. The intensity at $q = 0$ is given by:

$$I(0) = \frac{CM}{N_A}\left(\frac{m_pN_A}{M} - \rho_s\bar{\nu}_p\right)^2 \quad (2)$$

in which C is the sample concentration in NCP (w/v), M is the molecular weight of NCP, N_A is the Avogadro number, m_p is the number of electrons of the dry protein, ρ_s is the electronic density of the buffer, and $\bar{\nu}_p$ is the partial specific volume of the particle.

For a nearly spherical particle, the Guinier approximation is valid out to $qR_g = 1.3$. This range can even be slightly larger in the case of a moderately ellipsoidal particle. In practice, one obtains R_g and $I(0)$ by fitting $\ln I(q)$ as a function of q^2 for $q \leq 1.3/R_g$. However, for particles significantly different from a compact sphere, with some parts behaving as polymeric random chains, the validity of the Guinier approximation is restricted to very low q values and is thereby of no practical use. It has been shown in that case (Pérez et al., 2001) that the scattering function $I(q)$ is better described in the domain $q < 1.4/R_g$ by the Debye equation (Debye, 1947):

$$\frac{I(q)}{I(0)} = \frac{2}{x^2}(x - 1 + e^{-x}) \quad (3)$$

in which $x = q^2R_g^2$.

The radius of gyration provides information on the global shape of the particle. Additional information about the particle conformation can be obtained by calculating the distance distribution function $P(r)$, which is the Fourier transform of the scattering intensity $I(q)$. $P(r)$ is the distribution of intramolecular distances between scattering elements within the particle. $P(r)$ is equal to zero for distances r larger than the maximal diameter D_{max} of the particle. The $P(r)$ function for the different NCP solutions was determined using the program GNOM (Svergun et al., 1988). An estimate of the radius of gyration R_g can be derived from the distance distribution function.

In the case of interacting particles, the scattering patterns are modified by the effects of the positional correlations due to interactions. For spherical particles, the scattering intensity can be described by:

$$I(q,C) = I(q_{ideal}) \times S(q,C) \quad (4)$$

$I(q)_{ideal}$ is the scattering intensity in the absence of interaction and corresponds to the form factor of the particle. $S(q, C)$ is the structure factor, which characterizes the interactions between particles. This relationship has been shown to hold for particles displaying a moderate deviation from sphericity, although over limited ranges in concentration and momentum transfer q.

The intensity at the origin $I(0, C)$ is also modified, and its concentration dependence follows the relation:

$$I(0,C) = \frac{I(0)_{ideal}}{1 + 2A_2MC + 3A_3MC^2 + \ldots} \quad (5)$$

in which $I(0)_{ideal}$ is proportional to C according to Eq. 2 and $A_2, A_3, \ldots$ are the second, third,... virial coefficients, which represent interactions between two, three,... particles. These interactions result from the superposition of several components, in particular hard-core, repulsive Coulombic interactions and attractive Van der Waals forces. Net repulsive interactions lead to positive A_2 values and net attractive interactions to negative A_2 values. For a fixed NCP concentration, Eq. 5 indicates that net attractive/repulsive interactions enhance/decrease the intensity at the origin $I(0, C)$ above/below the value $I(0)_{ideal}$ characteristic of a solution of noninteracting particles. The intensities in the small angle region used for the determination of R_g are also modified and yield an apparent radius of gyration $R_g(C)$.

The virial coefficient A_2 can be evaluated by performing experiments at different particles concentrations for a fixed salt concentration. In practice, the third term, $3A_3MC^3$ and the following can be neglected if C is not too high (< 50 mg/ml). Then A_2 is proportional to the slope of $C/I(0, C)$ as a function of C. A plot of this quantity versus C also yields the "true" value of the intensity at the origin $I(0)_{ideal}$.

RESULTS

NCP_{165}

A first series of small angle x-ray scattering experiments was recorded with NCP_{165}, over a large range of monovalent salt concentrations C_s (10 mM to 1 M) and for different NCP concentrations C_{NCP} (5, 10, 50, 100 mg/ml).

Fig. 2 shows the effects of salts at a constant NCP concentration ($C_{NCP} = 5$ mg/ml). At $C_s = 10$ mM, a distinct peak is observed characteristic of net repulsive interactions (Ducruix et al., 1996; Tardieu et al., 1999). Increasing the ionic strength leads to the disappearance of this peak, which corresponds to the screening of the repulsive Coulombic interactions. The scattering curves obtained for some fixed salt concentrations C_s when varying the NCP concentration are shown on Fig. 3. In the absence of repulsive peak, the $I(0, C)$ values were extracted, using the Guinier approximation at very low q values. Only for $C_s = 1$ M, the Debye law

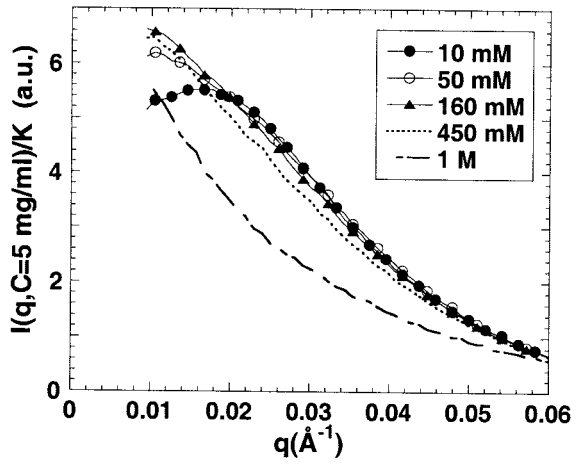

FIGURE 2 X-ray scattering curves recorded with NCP_{165} at a concentration of 5 mg/ml as a function of q ($q = (4\pi/\lambda)\sin\theta$, with 2θ being the scattering angle) for various salt concentrations. The $I(q, C = 5$ mg/ml) curves have been normalized by the electronic density contrast $K = \left(\frac{m_p N_A}{M} - \rho_s \bar{\nu}_p\right)^2$ (see Eq. 2), which depends on the salt concentration C_s via the electronic density ρ_s of the buffer.

is preferred to the Guinier approximation because the particle becomes partly unfolded, as explained in the following. The values of $I(0, C)$ were thus determined only for two NCP concentrations (5 and 10 mg/ml) for $C_s = 50$ mM and for three concentrations (5, 10, and 50 mg/ml) at higher salt concentrations. It follows that only an order of magnitude of the second order virial coefficient A_2 (Table 1) was deduced from the variation with C of $I(0, C)$ using Eq. 5. Increasing the salt concentration leads to the diminution of A_2, but even for high ionic strength, the values remain positive. Net interactions are always repulsive.

The data collected at 5 mg/ml have then been used to study the shape of the NCP as a function of the monovalent salt concentration (C_s ranging from 50 mM to 1 M) via the determination of the distance distribution function $P(r)$. For $C_s > 50$ mM, the effect of the interactions between particles at the NCP concentration $C_{NCP} = 5$ mg/ml can reasonably be neglected because the relative decrease $2A_2MC$ of the intensity at the origin $I(0, C)$ due to the effect of the interactions is smaller than 4%. Moreover the curves obtained for $C_{NCP} = 5$ and 10 mg/ml are nearly superimposed. Then the $I(q, C = 5$ mg/ml) curve can be considered as a good approximation of the spectrum $I(q)_{ideal}$ of a solution without interactions. For $C_s = 50$ mM, the $I(q, C = 5$ mg/ml) curve is slightly affected by the effect of interactions for the smallest q values ($q < 0.022$ Å^{-1}). Consequently the computing of the distance distribution function $P(r)$ as well as the determination of R_g from the Guinier approximation are performed using the q range $q > 0.022$ Å^{-1}. For $C_s < 50$ mM, the shape of the $I(q, C)$ curves is strongly affected by the interactions even for $C_{NCP} = 5$ mg/ml, and the determination of $P(r)$ is no more possible. Fig. 4 *A* gives the $P(r)$ functions computed with GNOM. As seen on these curves, the maximal extension of the particle D_{max} increases significantly with the salt concentration. The radius of gyration of the NCP, $R_g(P(r))$ has been calculated from the $P(r)$ functions for each C_s value. Results are given in Table 1, together with the R_g values obtained from the Guinier approximation ($C_s = 50$, 160, and 450 mM) or from

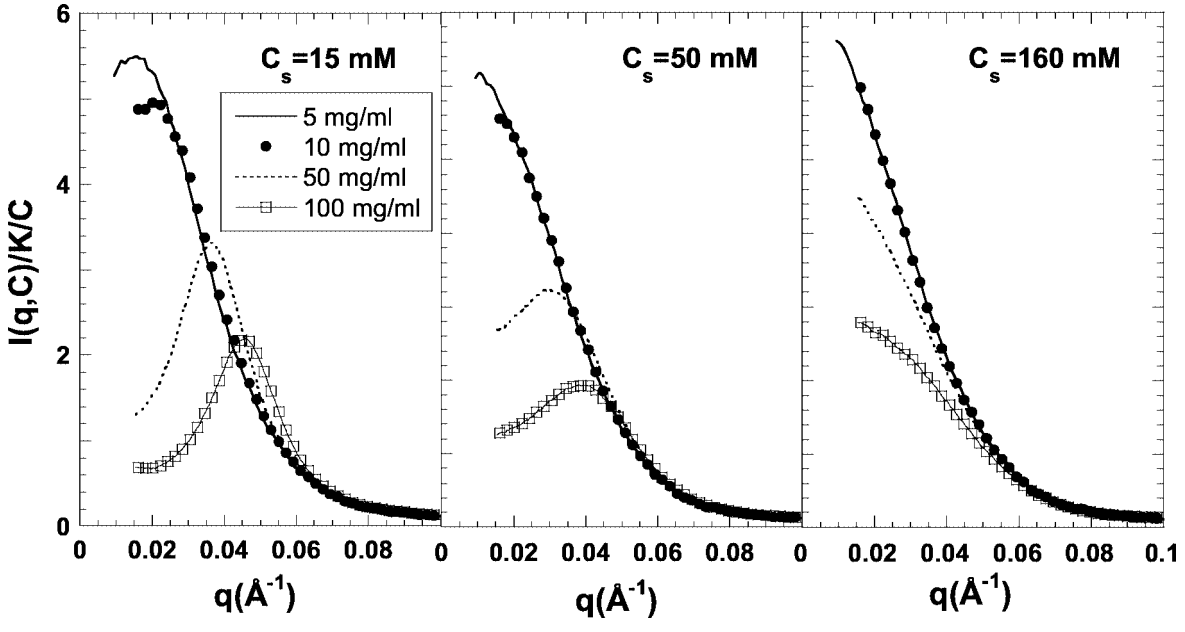

FIGURE 3 X-ray scattering curves recorded with NCP_{165} for different salt concentrations C_s and different NCP concentrations (indicated on the graphs). The $I(q, C)$ curves have been normalized by the NCP concentration C and by the electronic density contrast K.

TABLE 1 Values of the A_2 coefficient of NCP_{165}, determined for different salt concentrations C_s

NCP_{165}	C_s = 50 mM	C_s = 160 mM	C_s = 450 mM	C_s = 1 M
A_2 (ml mol g^{-2})	$6.10^{-5} \pm 2.10^{-5}$	$2.2.10^{-5} \pm 1.10^{-5}$	$1.7.10^{-5} \pm 1.10^{-5}$	$3.6.10^{-5} \pm 1.10^{-5}$
R_g (Guinier or Debye)	44.5 ± 0.3 Å	46.2 ± 0.2 Å	51.1 ± 0.5 Å	83.6 ± 3 Å
$R_g(P(r))$	44.8 ± 0.2 Å	47.1 ± 0.2 Å	51.4 ± 0.3 Å	86.0 ± 1.2 Å
D_{max}	138 ± 5 Å	171 ± 5 Å	185 ± 5 Å	335 ± 10 Å

The radii of gyration R_g calculated from the Guinier approximation (C_s = 50, 160, and 450 mM) or Debye law (C_s = 1 M) and from the $P(r)$ curves are also given, as well as the maximal extension of the particle D_{max}.

the Debye law (C_s = 1 M). Both sets of R_g values are in good agreement. For C_s = 50 and 160 mM, our R_g values are also in agreement with values reported previously (Greulich et al., 1985; Inoko et al., 1992). The R_g value increases significantly for $C_s \geq 450$ mM. Examination of the form factor of the particle in the whole q range brings more details on the shape of the particle. As seen on Fig. 4 *B*, the curve recorded at C_s = 450 mM differs significantly from the curves recorded at $C_s \leq 160$ mM for $q > 0.08$ $Å^{-1}$. In particular, the minimum around $q = 0.13$ $Å^{-1}$ is more shallow, suggesting a noticeable modification in the shape of the NCP. The curve is completely different at C_s = 1 M. This change in the form factor correlates with the change in R_g and can be attributed to a partial dissociation of the NCP in high salt conditions as already mentioned by several authors (Yager et al., 1989; Ausio et al., 1984, 1989; Krapunov et al., 1997; Ballestar et al., 2001). We did not intend to analyze further here the high C_s range leading to strong changes in the shape of the NCP and finally to the dissociation of DNA from the histone core. We instead chose to focus on the C_s range in which NCP integrity is preserved ($C_s \leq 200$ mM). In our experiments, a significant increase in the maximal diameter D_{max} was detected between 50 and 160 mM salt, well within this range.

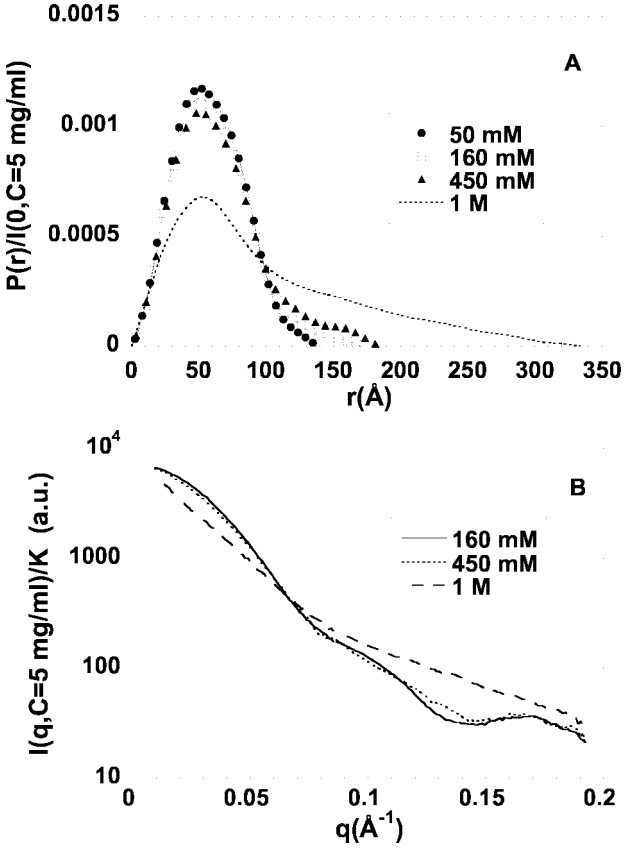

FIGURE 4 (*A*) Distance distribution function $P(r)$ calculated for various salt concentrations C_s at a fixed NCP_{165} concentration of 5 mg/ml. The $P(r)$ curves are scaled to the intensity at the origin $I(0, C = 5$ mg/ml). (*B*) X-ray scattering curves $I(q, C = 5$ mg/ml) normalized by the electronic density contrast K, recorded with NCP_{165} for three salt concentrations C_s: 160 mM, 450 mM, and 1 M. For clarity, the curves recorded for $C_s < 160$ mM are not represented because they are very similar to the curve obtained at C_s = 160 mM for $q \geq 0.05$ $Å^{-1}$. The unfolding of the particle is already clearly visible at C_s = 450 mM for $q > 0.085$ $Å^{-1}$. Intensities have been linearly smoothed using a moving window for clarity.

NCP_{145}

Using a second NCP population containing 145 bp, with a much narrower distribution (±3 bp), the range of salt concentration compatible with the integrity of the particles was explored in greater detail ($C_s \leq 200$ mM monovalent salt). Fig. 5 *A* shows x-ray scattering profiles in the small q range for different salt concentrations and C_{NCP} = 4 mg/ml. As previously described for NCP_{165}, the shielding of the repulsive electrostatic forces by addition of salts is still clearly observed. The curve recorded for C_s = 10 mM flattens for the smallest q values, which reveals the existence of net repulsive interactions. This behavior disappears for higher C_s concentrations. Above 50 mM, the curvature of the scattering pattern in the innermost part is even inverted, suggesting that the net interactions between NCP are there attractive.

For each salt concentration, the NCP concentration was varied from 0.5 to 4 or 8 mg/ml. Below 75 mM, the curves ln $I(q, C)$ are linear as a function of q^2 in the Guinier range ($qR_g \leq 1.3$) with the exception of the curve with a flat portion obtained for C_s = 10 mM and C_{NCP} = 4 mg/ml. Under these conditions, $I(q, C)$ can be extrapolated to q = 0, and the value of the second virial coefficient can be derived from Eq. 5 (Table 2). The A_2 value decreases progressively and becomes negative for $37.5 < C_s < 50$ mM, indicating a change from repulsive to attractive interactions. Above 75 mM, the Guinier plots (ln $I(q, C)$ versus

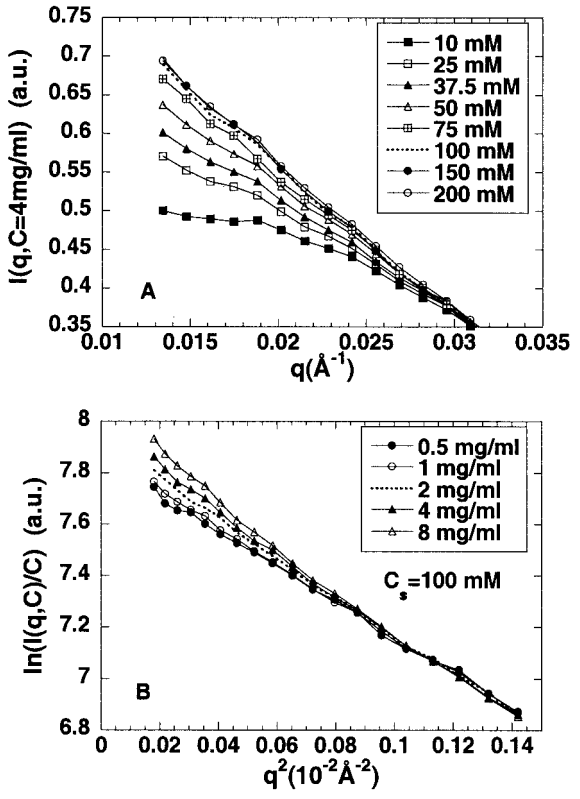

FIGURE 5 (*A*) X-ray scattering curves $I(q, C = 4$ mg/ml) recorded with NCP_{145} at a concentration of 4 mg/ml for various salt concentrations C_s between 10 and 200 mM. The variation of the electronic density contrast K over this C_s range being small (less than 3%), the $I(q, C)$ curves have not been normalized by K. (*B*) Guinier plots ($\ln(I(q, C))/C$) as a function of q^2) from data recorded at the salt concentration $C_s = 100$ mM for five NCP_{145} concentrations between 0.5 and 8 mg/ml. The $I(q, C)$ curves have been normalized by the NCP concentration C. For $C_{NCP} = 0.5$ and 1 mg/ml $\ln(I(q, C)/C)$ is perfectly linear as a function of q^2 in the Guinier range ($qR_g < 1.3$). For highest C_{NCP} values a slight deviation from the linearity is observed.

q^2) display a slight upward curvature at low q for the highest NCP concentrations (2, 4, and 8 mg/ml) (Fig. 5 *B*). This can be attributed either to attractive interactions in a monodisperse solution or to the formation of oligomers of core particles due to this attraction. As a consequence, no reliable extrapolation of the intensity $I(q, C)$ to the origin $I(0, C)$ can be performed above 100 mM in salt and for $C_{NCP} \geq 2$ mg/ml. It follows that the second virial coefficient A_2 cannot be determined using Eq. 5 in this range of salt concentration.

In keeping with these observations, the procedure used to derive a form factor free from interparticle interactions depends on salt concentration. At 10 mM salt, the interactions are sufficiently repulsive that the curves at 0.5 and 1 mg/ml display significant differences in the innermost region ($q < 0.03$ Å^{-1}). The data recorded at 0.5, 1, and 2 mg/ml were extrapolated to infinite dilution using a Zimm plot (Zimm, 1948). In the case of weak to moderate interactions, be they repulsive (25 and 37 mM) or attractive (50 and 75 mM), the differences between data recorded at 0.5 and 1 mg/ml were within experimental errors, and the curve recorded at 0.5 mg/ml was therefore considered to be unaffected by interparticle interactions. At higher salt concentration (100, 150, and 200 mM), attractive interactions were stronger, but the scattering patterns at 0.5 mg/ml did not significantly differ from the form factor at lower salt concentration (50 and 75 mM). Indeed, the value of the intensity extrapolated to the origin $I(0, C_{NCP} = 0.5$ mg/ml) is constant within error bars for all salt concentrations (Fig. 6 *D*). Here again, the most dilute sample ($C_{NCP} = 0.5$ mg/ml) was deemed free from any detectable interparticle effect. In a final step of data processing, the form factors were spliced with the corresponding high concentration data, which were unaffected by interparticle interactions at larger angles so as to improve the statistics in the outer region. The resulting patterns were used to calculate the distance distribution functions $P(r)$ shown in Fig. 6 *A*. Eliminating a few points in the innermost region, most sensitive to interparticle interactions did not significantly modify the $P(r)$ curves, confirming that the samples at $C_{NCP} = 0.5$ mg/ml are practically ideal.

Between 10 and 50 mM salt, the maximal extension D_{max} of the NCP increases from 137 ± 5 Å to 165 ± 5 Å before leveling off around that value up to a salt concentration of 200 mM (Fig. 6 *B*). R_g values were calculated using both the $P(r)$ curves and the Guinier formula. Both estimates show a similar increase over the same range of salt concentration (10–50 mM) and remain constant at higher concentration (Fig. 6 *C*). The slight difference between both sets of values is probably due to the fact that the angular range ($0.0147 \leq q \leq 0.0309$ Å^{-1}) used to determine the radius of gyration from the Guinier approximation does not reach small enough q values, thereby yielding a slight underestimate of the R_g value. Finally, it must be emphasized that the increase in R_g and D_{max} are observed at C_s values (10–50 mM) lower than the onset of strong attractive interactions (≥100 mM), susceptible to cause the formation of oligomers. Thereby these variations in R_g and D_{max} cannot be attributed to aggregation as confirmed by the constancy of $I(O, C = 5$ mg/mP) (Fig. 6 *D*).

TABLE 2 Values of the A_2 coefficient, determined for different salt concentrations C_s with NCP_{145}

NCP_{145}	$C_s = 10$ mM	$C_s = 25$ mM	$C_s = 37.5$ mM	$C_s = 50$ mM	$C_s = 75$ mM
A_2 (ml mol g^{-2})	$15.10^{-5} \pm 2.10^{-5}$	$4.5.10^{-5} \pm 1.5.10^{-5}$	$3.10^{-6} \pm 3.10^{-6}$	$-5.10^{-6} \pm 5.10^{-6}$	$-2.10^{-5} \pm 1.10^{-5}$

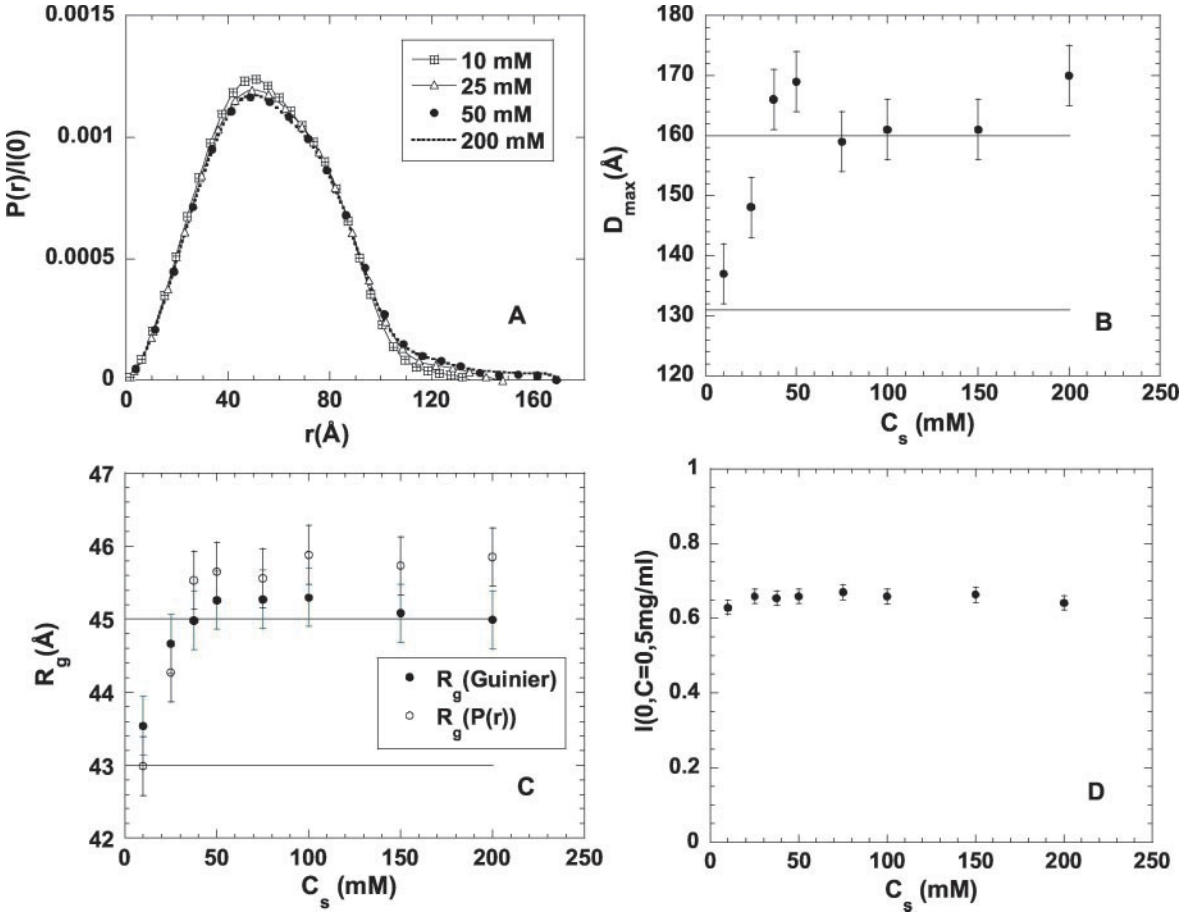

FIGURE 6 Data obtained for NCP_{145} as a function of the salt concentration. (*A*) Distance distribution function $P(r)$ calculated for four different salt concentrations (C_s) from the $I(q)$ curves compiled in the following manner: when $q \leq 0.05$ Å^{-1}, $I(q, C = 0.5$ mg/ml) was used; when $q > 0.05$ Å^{-1}, $I(q, C = 4$ or 8 mg/ml) was used. The $P(r)$ curves are scaled to the intensity at the origin $I(0)$. (*B*) Maximal extension values D_{max} plotted as a function of the salt concentration C_s. Both solid lines correspond to the D_{max} values 131 and 160 Å obtained from the $P(r)$ curves calculated for the nucleosome core particle modeled with the condensed or extended tails, respectively. (*C*) Variation of the radius of gyration R_g of NCP_{145} as a function of the salt concentration C_s. R_g (Guinier) comes from the Guinier approximation; R_g ($P(r)$) was deduced from the calculation of the $P(r)$ function. Both solid lines correspond to the R_g values 43 and 45 Å obtained from the $I(q)$ curves calculated for the nucleosome core particle modeled with the condensed or extended tails, respectively. (*D*) Intensity extrapolated to the origin $I(0, C = 0.5$ mg/ml).

DISCUSSION

The interactions between isolated nucleosome core particles have been studied with NCP_{145} and NCP_{165}. They were carefully analyzed with NCP_{145} in the range of salt concentration where particle integrity is preserved: the second virial coefficient A_2, which is positive in low salt conditions becomes negative above 50 mM salt. For both types of NCP, Coulombic repulsive interactions between particles are screened by salt, but the salt concentration required to achieve complete screening is shifted to higher values for NCP_{165}. Moreover, in the latter case, net interactions never become attractive whatever the salt concentration (up to 1 M monovalent salt) (Table 1), in contrast to the attraction observed for NCP_{145} above 50 mM salt. Thus, at a salt concentration fixed to $C_s = 150$ mM, net interactions are repulsive for NCP_{165} and attractive for NCP_{145}. Nevertheless, our A_2 values must be compared with the A_2 value calculated for a hard sphere potential (A_{2hs}). $A_{2hs} = 4\nu N_A/M^2$, in which ν is the volume of the particle. With an R_g value in the range from 43 Å to 45 Å, A_{2hs} is comprised between 0.40 and 0.46 10^{-4} mol ml g^{-2}. In the two series of experiments, the A_2 values are lower than the A_{2hs} values at C_s 150 mM (Fig. 7). The balance of all interactions, with the exception of hard sphere interaction, is therefore attractive for both kinds of particles NCP_{145} and NCP_{165}, with a higher attractive potential in the case of NCP_{145}.

The difference in the salt concentration required to achieve complete screening of electrostatic repulsion can be attributed to differences between the charge of the particles. The DNA length associated to the histone octamer is significantly different in the two series of experiments (165 vs 145 bp). The 20-bp-longer DNA fragments brings 40 addi-

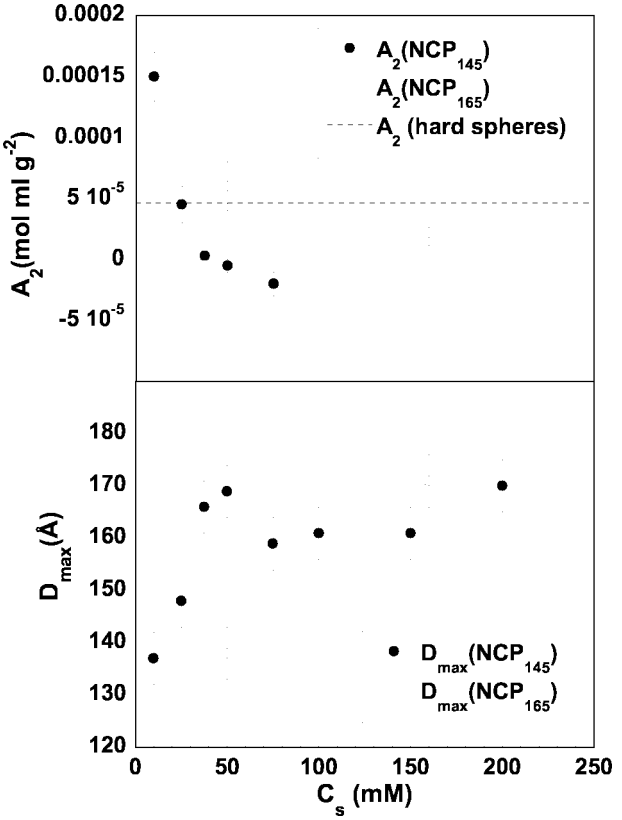

FIGURE 7 Variation of A_2 and D_{max} as a function of salt concentration C_s. Data recorded with NCP_{145} ●; data recorded with NCP_{165} ○.

tional negative charges (each phosphate group carries a negative charge). With 220 positively charged amino acids (Lys and Arg) and 74 negatively charged amino acids (Glu and Asp) in the core, the structural charge of the isolated nucleosome core particles comes to 144 e^- for NCP_{145} and 184 e^- for NCP_{165}. These extra two turns of DNA carried by the NCP_{165} could explain differences in the A_2 behavior. Another source of A_2 differences may come from differences in the charges carried by the histones: 1) differences between calf and chicken amino acid sequences can be disregarded because they do not involve charged amino acids (Van Holde, 1988). 2) Posttranslational modifications, namely acetylation and phosphorylation of the tails, could also produce significant changes in the charges of the particles. However, this effect is likely to be negligible because our preparation methods produce only poorly acetylated particles.

Similar screening effects of Coulombic interactions by salt were analyzed in solutions of proteins. A transition from net repulsive to net attractive interactions was observed with small molecular weight proteins, namely lysozyme and γ-crystallins (Tardieu et al., 1992; Muschol and Rosenberger, 1995; Ducruix et al., 1996). By adding salt, the repulsive electrostatic interactions between particles are screened, and short distance attractive interactions are revealed. The nature of these interactions remains to be determined. As far as we know, transitions from net repulsive to net attractive interactions have not yet been reported with large proteins analyzed so far (Budayova et al., 1999; Bonneté et al., 2001; Petsev and Vekilov, 2000).

The cylindrical shape of the nucleosome core particle, combined with its heterogeneous distribution of charges creates multiple possibilities of interactions that may be responsible for this original behavior. Osmometry measurements performed over the same range of monovalent ions concentrations also reveal the presence of these attractive interactions between isolated NCP. We suspect the histone tails to be involved in these attractive interactions (Mangenot et al., 2002). Anisotropic interactions may occur between top and bottom faces or between lateral sides of NCP, as revealed by the supramolecular organization of the particles at concentrations above 100 mg/ml (Leforestier et al., 2001).

Special care has been taken to determine the form factors of NCP_{145} free from any interparticle effect, thereby allowing us to study the variation of the shape of the nucleosome core particles with salt concentration. The general shape of the form factor as well as the value of the radius of gyration display only slight changes when the monovalent salt concentration is increased from 10 to 200 mM. In contrast, the maximal extension of the particle D_{max} increases significantly from 137 ± 5 Å to 165 ± 5 Å when C_s rises from 10 to 50 mM and remains at this plateau value for salt concentrations above 50 mM. The tail of the $P(r)$ function for r values higher than 130 Å observed at high salt concentration shows that the number of large distances inside the particle is small. Because the concomitant variation of the radius of gyration is weak, we propose that the increase of D_{max} reflects only the extension of the histone tails without significant change of the shape of the rest of the particle. To test this hypothesis, a nucleosome core particle was constructed with either extended or condensed tails (Fig. 8, *A* and *B*) starting from the crystallographic coordinates recently published by Harp et al. (2000) (PDB file 1eqz). NCPs were prepared from native chicken histone octamer cores and a palindromic DNA. In their study, the structure of parts of the N-terminal region of each histone and of the C-terminal region of H2A could not be determined. We therefore undertook to add the missing 102 residues of these tails, in a random coil conformation, using the modeling tools from Turbo-FRODO (Roussel and Cambillau, 1989). Two models were built, one designated as the "extended" conformation in which the tails are freely extended away from the particle, whereas they are located close to the DNA surface in the other, "compact" conformation. These two conformations were built to account for the dimensions of the particles with no claim to describe the exact conformation of the tails. The polypeptide chains were placed in an arbitrary position well exposed to the solvent, because their high mobility makes them likely to explore a fairly large

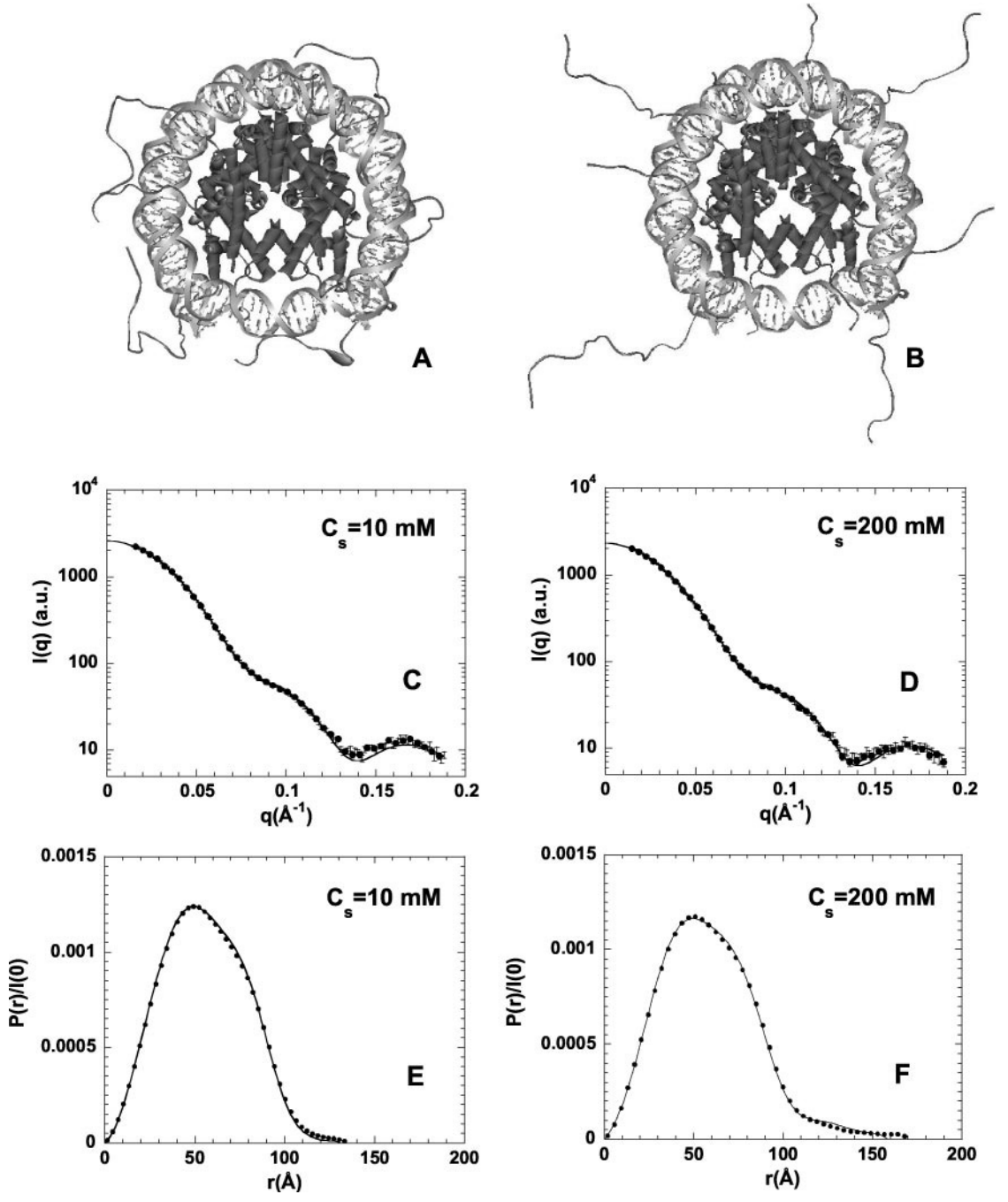

FIGURE 8 NCP models in the "compact" (*A*) and "extended" (*B*) conformations. (*C* and *D*) Scattering patterns of NCP for C_s = 10 and 200 mM, respectively. Dots, Experimental data; continuous lines, calculated patterns from crystallographic data corresponding to the "compact" and "extended" conformations (*A*) and (*B*). (*E* and *F*) Distance distributions functions $P(r)$ for C_s = 10 and 200 mM, respectively. Dots, Experimental data; Continuous lines, calculated $P(r)$ curves.

volume around the core particle. Care was just taken to build the tails with no repeated features in shape and orientation so as not to introduce any element of symmetry, albeit very crude, which could have added some artifactual oscillations to the calculated scattering patterns. Their contribution to scattering is that of an average conformation. In keeping with this low resolution approach, no attempt was made to introduce the α-helical conformation of the tails condensed onto DNA (Baneres et al., 1997; Wang et al., 2000). Both conformations shown on Fig. 8, *A* and *B*, must be considered as representative of each conformational space. The experimental curve $I(q)$ obtained for NCP_{145} at

C_s = 10 mM was fitted by the curve representative of an ideal solution of NCP in the modeled "compact" conformation, using the program CRYSOL (Svergun et al., 1995). This program uses only two free parameters: the average displaced solvent volume per atomic group and the contrast of the hydration shell. The fit yields an excellent agreement (Fig. 8 *C*) for a relative density of the hydration layer of the order of 1.15. The R_g value derived from the calculated curve $I(q)$ is 43 Å, very close to the experimental value. The $P(r)$ curve deduced from the calculated curve is shown on Fig. 8 *E* and gives a D_{max} value of 131 Å. Similar fits of the experimental curves obtained between 50 and 200 mM have been performed using the modeled "extended" conformation. An excellent agreement between experimental and calculated curves is also observed (Fig. 8, *D* and *F*), whereas the value of the relative density of the hydration layer is found to be 1.16, practically identical to the value found for the compact particle. R_g and D_{max} values deduced from the calculated curve are respectively 45 and 160 Å. Note that the D_{max} value extracted from the $P(r)$ distribution corresponds to the maximal overall diameter of the particle only in the "compact" conformation. This D_{max} value is significantly lower than the maximal extension in the "extended" conformation, as easily seen on the model representations in Fig. 8. This difference comes from the very low fraction of the scattering mass present in the tails compared with the central core of the nucleosome core particle. The tails contribute only marginally to the scattering intensity. In the extended conformation, the largest distances (separating the extremities of the tails) inside the particle contribute too few vectors to be detected in the calculated scattering pattern. Nevertheless, the important result is that experimental and theoretical D_{max} values coincide.

The tails carry numerous Lys and Arg positively charged amino acids, which are able to interact with the negative charges carried by the phosphate groups of the DNA molecule when the Coulombic interactions are not screened. When increasing the ionic strength, these interactions are strongly shielded, leading to the unfolding of the tails and to their extension in the solution. This behavior agrees with the theoretical calculations of Clark and Kimura (1990) who, using Manning theory of counterions condensation, calculated that all or nearly all of the lysine and arginine residues in the tails are bound to DNA in the NCP at low salt. Based on the nuclear magnetic resonance experiments performed years ago on isolated NCP, oligonucleosomes (Cary et al., 1978; Hilliard et al., 1986; Smith and Rill, 1989) and chromatin (Walker, 1984) there is quite an agreement about the fact that the tails would be bound to DNA in low salt and become released and mobile when the ionic strength is increased above 0.2 to 0.4 M NaCl. However, above 0.2 M, the extension of the tails is not really uncoupled from the other salt-induced changes, which do not involve histone tails because they occur equally well whether histone tails are present or not (Ausio et al., 1989). Our experimental results show that the extension of the tails occurs much below 0.2 M NaCl, over a small range of salt concentration and that this process can be separated from the other salt-induced conformational changes of the nucleosome core particle: 1) separation of DNA from the proteins of the core, which may occur at very low (< a few mM NaCl) or very high salt concentration (> 0.8 M NaCl) (Ausio et al., 1984; Yager et al., 1989). The dissociation of DNA from histones is negligeable in our experiments. 2) Reversible changes in the conformation of the particle occur in the range 0.2 to 0.8 M NaCl (Ausio and Van Holde, 1986; Dong et al., 1990). We observe these changes in the form factor and in the radius of gyration but at higher salt concentrations (450 mM), well after the extension of the tails. Ballestar and Franco (1997), using the accessibility of the glutamine residues to monitor conformational changes of the tails, also reported that the extension process starts at very low salt concentration, below 50 mM. Moreover, they interpreted their data as a two-step process. From our experiments, we cannot say whether there are intermediate states in the extension process or determine the order in which the different tails extend.

Interestingly, the extension of the tails that we observe above 50 mM salt for NCP_{145}, without any other conformational change of the particle, mimics the effects induced by the acetylation of the histones. The basic structure of the nucleosome remains unchanged (Ausio and Van Holde, 1986; Imaï et al., 1986; Libertini et al., 1988), whereas interactions between the tails and nucleosomic DNA are lowered as a consequence of the decrease in the positive charges at the N terminal regions of the tails (Ausio et al., 1989; Oliva et al., 1990). The hyperacetylated cores have a lower sedimentation coefficient than control particles over a wide range of salt concentration, and only low levels of acetylation are necessary to produce this effect (Ausio and Van Holde, 1986).

We also followed the extension of the histone tails in the experiments performed with NCP_{165}. Nevertheless, the salt concentration C_s at which this extension is detected is shifted toward higher values (between 50 and 150 mM). We assume that this shift in salt concentration is due to the longer length of the DNA fragments associated to the particles, which brings extra negative charges to be screened. This would also explain why Mutskov et al. (1998), using ultraviolet laser-induced histone-DNA cross-linking, observed the extension of the tails at even higher salt concentration, between 0.2 and 0.5 M NaCl: in their experiments, the nucleosomal DNA was 180 bp long. In our two series of experiments (NCP_{145} and NCP_{165}), the extension of the tails is detected at the salt concentration C_s for which the A_2 values become smaller than the hard sphere second virial coefficient A_{2hs}. It follows that changes in the interactions between particles and modifications of their conformation occurring when the salt concentration is increased can both

be understood as consequences of a similar screening effect of Coulombic interactions. At low salt, nucleosome core particles, which are negatively charged, interact via net repulsive interactions, whereas interactions between negatively charged DNA and positively charged tails are net attractive. Addition of salt simultaneously screens repulsive interactions between NCP and attractive interactions between tails and DNA inside the NCP. The intraparticle and interparticles phenomena are thus coupled. From a functional point of view, the coupling between these two effects is of importance in the regulation of gene activity and namely transcription. Indeed, during these last years, pieces of a real "chromatin modifying machinery" such as acetyl transferases and deacetylases were discovered, which act by modifying the charge distribution carried by the histone tails, thereby modulating the accessibility of chromatin to the transcription machinery.

We thank Ariel Prunell for many helpful discussions, especially on the methodological aspects of nucleosome preparation. We also thank Eric Raspaud for fruitful discussions.

REFERENCES

Ausio, J., F. Dong, and K. E. Van Holde. 1989. Use of selectively trypsinized nucleosome core particles to analyze the role of the histone "tails" in the stabilization of the nucleosome. *J. Mol. Biol.* 206:451–463.

Ausio, J., D. Seger, and H. Eisenberg. 1984. Nucleosome core stability and conformational change: effect of temperature, particle and NaCl concentrations, and crosslinking of histone H3 sulfhydryl groups. *J. Mol. Biol.* 176:77–104.

Ausio, J., and K. E. Van Holde. 1986. Histone hyperacetylation: its effects on nucleosome conformation and stability. *Biochemistry.* 25:1421–1428.

Ballestar, E., M. Boix-Chornet, and L. Franco. 2001. Conformational changes in the nucleosome followed by the selective accessibility of histone glutamines in the transglutaminase reaction: effetcs of ionic strength. *Biochemistry.* 40:1922–1929.

Ballestar, E., and L. Franco. 1997. Use of transglutaminase reaction to study the dissociation of histone N-terminal tails from DNA in nucleosome core particles. *Biochemistry.* 36:5963–5969.

Baneres, J. L., A. Martin, and J. Parello. 1997. The N tails of histones H3 and H4 adopt a highly structured conformation in the nucleosome. *J. Mol. Biol.* 273:503–508.

Bonneté, F., D. Vivarès, C. Robert, and N. Colloc'h. 2001. Interactions in solution and crystallisation of *Aspergillus flavus* urate oxidase. *J. Crystal Growth.* In press.

Budayova, M., F. Bonneté, A. Tardieu, and P. Vachette. 1999. Interactions in solution of a large oligomeric protein. *J. Crystal Growth.* 196: 210–219.

Cary, P. D., T. Moss, and E. M. Bradbury. 1978. High resolution proton-magnetic resonance studies of chromatin core particles. *Eur. J. Biochem.* 89:475–482.

Clark, D. J., and T. Kimura. 1990. Electrostatic mechanism of chromatin folding. *J. Mol. Biol.* 211:883–896.

De Lucia, F., M. Alilat, A. Sivolob, and A. Prunell. 1999. Nucleosome dynamics: III Histone tail-dependant fluctuation of nucleosomes between open anc closed DNA conformations: implications for chromatin dynamics and the linking number paradox: a relaxation study of mononucleosomes on DNA minicircles. *J. Mol. Biol.* 285:1101–1119.

Debye, P. 1947. *J. Phys. Colloid. Chem.* 51:18–32.

Dong, F., C. Nelson, and J. Ausio. 1990. Analysis of the changes in the structure and hydration of the nucleosome core particle at moderate ionic strengths. *Biochemistry.* 29:10710–10716.

Ducruix, A., J. P. Guilloteau, M. Riès-Kautt, and A. Tardieu. 1996. Protein interactions as seen by solution X-ray scattering prior to crystallogenesis. *J. Crystal Growth.* 168:28–39.

Fletcher, T. M., and J. C. Hansen. 1995. Core histone tails domains mediate oligonucleosome folding and nucleosomal DNA organization through distinct molecular mechanisms. *J. Biol. Chem.* 270:25359–25362.

Fletcher, T. M., and J. C. Hansen. 1996. The nucleosomal array: structure/function relationships. *Crit. Rev. Eukaryot. Gene Expr.* 6:149–188.

Garcia-Ramirez, M., F. Dong, and J. Ausio. 1992. Role of the histone "tails" in the folding of oligonucleosomes depleted of histones H1. *J. Biol. Chem.* 267:19587–19595.

Greulich, K. O., J. Ausio, and H. Eisenberg. 1985. Nucleosome core particle structure and structural changes in solution. *J. Mol. Biol.* 186: 167–173.

Guinier, A., and G. Fournet. 1955. Small Angle Scattering of X-Rays. Wiley, New York.

Harp, J. M., B. L. Hanson, D. E. Timm, and G. J. Bunick. 2000. Asymmetries in the nucleosome core particle at 2.5 Å resolution. *Acta Cryst. D.* 56:1513–1534.

Hilliard, P. R., R. M. Smith, and R. L. Rill. 1986. Natural abundance carbon-13 nuclear magnetic resonance studies of histone and DNA dynamics in nucleosome cores. *J. Biol. Chem.* 261:5992–5998.

Imaï, B. S., P. Yau, J. P. Baldwin, K. Ibel, R. P. May, and E. M. Bradbury. 1986. Hyperacetylation of core histones does not cause unfolding of nucleosomes. *J. Biol. Chem.* 261:8784–8792.

Inoko, Y., M. Yamamoto, S. Fujiwara, and T. Ueki. 1992. X-ray scattering study of the shape of the DNA region in nucleosome core particle with synchrotron radiation. *J. Biochem.* 111:310–316.

Kornberg, R. D., and Y. Lorch. 1999. Twenty-five years of the nucleosome, fundamental particle of the eukaryote chromosome. *Cell.* 98: 285–294.

Leforestier, A., J. Dubochet, and F. Livolant. 2001. Bilayers of nucleosome core particles. *Biophys. J.* 81:2414–2421.

Leforestier, A., and F. Livolant. 1997. Liquid crystalline ordering of nucleosome core particles under macromolecular crowding conditions: evidence fora discotic columnar hexagonal phase. *Biophys. J.* 73: 1771–1776.

Libertini, L. J., K. E. Van Holde, and E. W. Small. 1988. Histone hyperacetylation: its effects on nucleosome core particle transitions. *Biophys. J.* 53:477–487.

Livolant, F., and A. Leforestier. 2000. Chiral discotic columnar germs of nucleosome core particles. *Biophys. J.* 78:2716–2729.

Lüger, K., A. W. Mäder, R. K. Richmond, D. F. Sargent, and T. J. Richmond. 1997. Crystal structure of the nucleosome core particle at 2.8 Å resolution. *Nature.* 389:251–260.

Lüger, K., and T. J. Richmond. 1998. The histone tails of the nucleosome. *Curr. Opin. Genet. Dev.* 8:140–146.

Mutskov, V., D. Gerber, D. Angelov, J. Ausio, J. Workman, and S. Dimitrov. 1998. Persistent interactions of core histone tails with nucleosomal DNA following acetylation and transcription factor binding. *Mol. Cell. Biol.* 18:6293–6304.

Muschol, M., and F. Rosenberger. 1995. Interactions in undersaturated and supersaturated lysozyme solutions: static and dynamic light scattering results. *J. Chem. Phys.* 103:10424–10432.

Oliva, R., D. P. Bazett-Jones, L. Locklear, and G. H. Dixon. 1990. Histone hyperacetylation can induce unfolding of the nucleosome core particle. *Nucleic Acids Res.* 18:2739–2747.

Pérez, J., P. Vachette, D. Russo, M. Desmadril, and D. Durand. 2001. Heat induced unfolding of neocarzinostatin, a small all-β protein investigated by small angle x-ray scattering *J. Mol. Biol.* 308:721–743.

Petsev, D. N., and P. G. Vekilov. 2000. Evidence for non-DLVO hydration interactions in solutions of the protein apoferritin. *Phys. Rev. Lett.* 84:1339–1342.

Richmond, T. J., J. T. Finch, B. Rushton, D. Rhodes, and A. Klug. 1984. Structure of the nucleosome core particle at 7 Å resolution. *Nature.* 311:532–537.

Roussel, A., and C. Cambillau. 1989. TURBO-FRODO. *In* Silicon Graphics Geometry Partners Directory 86. Silicon Graphics, Mountain View, CA.

Smith, R. M., and R. L. Rill. 1989. Mobile histone tails in nucleosomes. *J. Biol. Chem.* 264:10574–10581.

Svergun, D. I., C. Barberato, and M. H. J. Koch. 1995. CRYSOL: a program to evaluate X-ray solution scattering of biological macromolecules from atomic coordinates. *J. Appl. Cryst.* 28:768–773.

Svergun, D., A. Semenyuk, and L. A. Feigin. 1988. Small-angle-scattering-data treatment by the regularization method. *Acta Crystallogr.* A44: 244–250.

Tardieu, A., A. LeVerge, M. Malfois, F. Bonneté, S. Finet, M. Riès-Kautt, and L. Belloni. 1999. Proteins in solution: from x-ray scattering intensities to interaction potentials. *J. Crystal Growth.* 196:193–203.

Tardieu, A., F. Vérétout, B. Krop, and C. Slingsby. 1992. Protein interactions in the calf eye lens: interactions between β-crystallins are repulsive whereas in γ-crystallins they are attractive. *Eur. Biophys. J.* 21:1–12.

Van Holde, K. E. 1988. Chromatin. *In* Springer Series in Molecular Biology. A. Rich, series editor. Springer Verlag, New York.

Walker, I. O. 1984. Differential dissociation of histone tails from core chromatin. *Biochemistry.* 23:5622–5628.

Wang, X., S. C. Moore, M. Laszckzak, and J. Ausio. 2000. Acetylation increases the α-helical content of the histone tails. *J. Biol. Chem.* 2765:35013–35020.

Widom, J. 1986. Physicochemical studies of the folding of the 100 Å nucleosome foilament into the 300 Å filament. *J. Mol. Biol.* 190: 411–424.

Yager, T. D., C. T. McMurray, and K. E. Van Holde. 1989. Salt-induced release of DNA from nucleosome core particles. *Biochemistry.* 28: 2271–2281.

Zimm, B. H. 1948. The scattering of light and the radial distribution function of high polymer solutions. *J. Chem. Phys.* 16:1093–1116.